arXiv:1202.4799v1 [cond-mat.str-el] 22 Feb 2012

Alternating spin chains coupled by frustrated interactions in the multiferroic $FeTe_2O_5Br$

M. Pregelj,[1,2] H. O. Jeschke,[3] H. Feldner,[3] R. Valentí,[3] A. Honecker,[4] T. Saha-Dasgupta,[5] H. Das,[5] S. Yoshii,[6] T. Morioka,[6] H. Nojiri,[6] H. Berger,[7] A. Zorko,[1,8] O. Zaharko,[2] and D. Arčon[1,9]

[1]*Institute "Jožef Stefan", Jamova c. 39, SI-1000 Ljubljana, Slovenia*
[2]*Laboratory for Neutron Scattering, PSI, CH-5232 Villigen, Switzerland*
[3]*Institut für Theoretische Physik, Goethe-Universität Frankfurt am Main, 60438 Frankfurt am Main, Germany*
[4]*Institut für Theoretische Physik and Fakultät für Mathematik und Informatik, Georg-August-Universität Göttingen, Germany*
[5]*Satyandranath Bose National Centre for Basic Sciences, Kolkata 700098, India*
[6]*Institute for Materials Research, Tohoku University, Sendai 980-8577, Japan*
[7]*École Polytechnique Fédérale de Lausanne, Switzerland*
[8]*EN–FIST Centre of Excellence, Dunajska 156, SI-1000 Ljubljana, Slovenia*
[9]*Faculty of mathematics and physics, University of Ljubljana, Jadranska c. 19, SI-1000 Ljubljana, Slovenia*

(Dated: February 16, 2012)

Density functional theory calculations performed for the multiferroic $FeTe_2O_5Br$ reveal surprisingly strong super-superexchange pathways through Fe-O-Te-O-Fe bridges, implying that the magnetic lattice must be treated as a system of alternating Fe chains coupled by frustrated interactions. We find firm support for this model in the magnetization and the antiferromagnetic resonance measurements as well as in the matching of the incommensurate magnetic vector. Its peculiar temperature dependence is explained by interchain exchangestriction being responsible for the emergent net electric polarization.

Frustrated low-dimensional spin systems exhibit a plethora of exotic magnetic ground states, which are an exciting challenge both for theorists and experimentalists [1]. Since quantum fluctuations enhanced by frustration tend to destabilize classically ordered states, such systems often develop complex orders with broken inversion symmetry thus fulfilling the fundamental condition for multiferroicity. This can lead to strong magnetoelectric (ME) coupling [2–4], most spectacularly observed as reversal of the electric polarization with the magnetic field [5]. So far, strong ME coupling has been almost exclusively associated with transition metal (TM) oxides. However, unconventional magnetic ground states [6] and multiferroicity [7, 8] have been recently found also in TM tellurite halides, where TM ions are coupled through complex exchange pathways involving tellurium polyhedra [9, 10]. Due to the structural complexity of this family a microscopic mechanism of the ME coupling has yet to be established.

As a prominent member of the TM tellurite halide multiferroics we refer here to $FeTe_2O_5Br$ [8, 9], which adopts a layered structure with crystal layers of $[Fe_4O_{16}]^{20-}$ tetramer clusters connected via Te^{4+} ions [Fig. 1(a)]. The negative Curie-Weiss temperature $T_{CW} = -98$ K implies strong antiferromagnetic (AFM) interactions between the Fe^{3+} ($S = 5/2$) moments, while the system develops long-range magnetic order at a considerably lower temperature $T_{N1} = 11\,\mathrm{K}$ [8, 9, 11]. Only 0.5 K below, at $T_{N2} = 10.5\,\mathrm{K}$, the second transition to a predominantly amplitude modulated magnetic ground state with the incommensurate (ICM) magnetic vector $\mathbf{q}_{ICM} = (\frac{1}{2}\,0.463\,0)$ [8] occurs and is accompanied by a spontaneous electric polarization pointing perpendicular to the magnetic moments and to $\mathbf{q}_{ICM}$. The magnetic susceptibility was explained by assuming dominant interactions within tetramers [9]. However, the tetramer model cannot explain the observed ICM magnetic structure, essential for the ME effect in this system. The complexity of the TM tellurite halides arises from the exchange pathways that may involve several atoms. This makes their determination much less intuitive [12–14] as opposed to the TM oxides, where dominant TM-O-TM exchange interactions can be intuitively guessed from the bonding an-

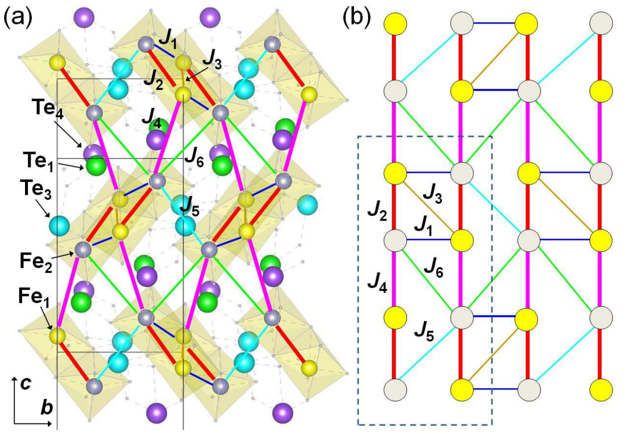

FIG. 1. (Color online) (a) Crystal structure of $FeTe_2O_5Br$ along the *bc* plane where light yellow polyhedra denote $[Fe_4O_{16}]^{20-}$ tetramer units. For clarity only Fe and Te atoms are shown. (b) The DFT magnetic exchange network, where the strongest J_2 and J_4 (thick lines) form alternating spin chains coupled by weaker frustrated interactions (thin lines). Marked unit cell contains 8 magnetic Fe^{3+} ions.

TABLE I. Exchange, J_i, and easy-plane anisotropy, D, parameters given in units of Kelvins and of J_2 as calculated by DFT calculations for GGA+U, U=0, 3 eV and 5 eV. The last column correspond to the parameters obtained from magnetic ground state minimization and used for the AFMR simulation (AFMR + GS min).

J_i	**GGA**		**GGA+U** $U = 3$**eV**		**GGA+U** $U = 5$**eV**		**AFMR +** **GS min**	
	(K)	(J_2)	(K)	(J_2)	(K)	(J_2)	(K)	(J_2)
J_1	30.5	0.60	13.4	0.46	6.86	0.35	8.9	0.47
J_2	51.1	1	29.2	1	19.6	1	19.0	1
J_3	17.3	0.34	9.7	0.33	6.66	0.34	6.2	0.324
J_4	35.3	0.69	18.1	0.62	11.56	0.59	11.8	0.62
J_5	4.0	0.078	1.2	0.042	-0.02	-0.001	0.8	0.042
J_6	15.5	0.30	7.9	0.27	5.10	0.26	5.0	0.265
D	-	-	-	-	-	-	0.18	0.0095

gles [15, 16]. Therefore, additional experimental and theoretical investigations are needed to determine the magnetic exchange network, which should unveil the microscopic origin of the complicated magnetic order as well as its coupling to the electric polarization.

In this letter, we report on density functional theory (DFT) calculations for $FeTe_2O_5Br$, which surprisingly reveal that long Fe-O-Te-O-Fe super-superexchange bridges are stronger than some shorter and more direct Fe-O-Fe ones. Consequently, a quasi-one-dimensional model of alternating AFM Fe chains weakly coupled by frustrated two-dimensional interactions has been derived and verified by experiments. In this picture, the ICM magnetic structure appears naturally. Considering the fact that the ICM component of the magnetic vector along the crystallographic b-axis, q^y_{ICM}, shows a similar temperature dependence as the electric polarization [11], we conclude that the microscopic origin of the ME effect is the magnetostriction of the interchain Fe-O-Te-O-Fe exchange pathways. These involve Te^{4+} ions hosting easily polarizable lone-pair electrons.

Density Functional Theory.– The underlying Heisenberg Hamiltonian parameters for $FeTe_2O_5Br$ (Table I) were determined by total energy calculations. A full potential local orbital basis set [17] and generalized gradient approximation (GGA) as well as GGA+U functionals were used. The Hubbard parameter U was chosen as 3 and 5 eV to take into account the intra-atomic Coulomb interactions. The obtained network of exchange interactions (Fig. 1) was checked for consistency by N^{th}-order muffin-tin orbital downfolding [18] calculations.

The six considered exchange couplings are all antiferromagnetic. As expected, the intracluster (within a tetramer) Fe-O-Fe exchange J_2 is the strongest. Strikingly, the second strongest exchange is not the remaining intracluster Fe-O-Fe exchange J_1, but rather the intercluster super-superexchange interaction J_4, mediated through the Fe-O-Te-O-Fe bridges. This result discloses that in tellurite halides the super-superexchange interactions through long bridges involving Te^{4+} ions are important and should not be neglected on the basis of simplified structural arguments. The two dominant couplings, J_2 and J_4, thus effectively form alternating Fe^{3+} spin chains. The rest of the considered exchange interactions are weaker and provide frustrated interchain interactions as shown in Fig. 1. We note that the DFT results leave some freedom concerning the overall energy scale, but the ratios of J_i's are expected to be subject only to small errors [19]. However, the relative sizes of J_i's are somewhat dependent on the chosen value of U, with J_1 and J_5 showing the highest sensitivity. Thus, we suspect that they could be modified by very small lattice distortions anticipated at the ME transition.

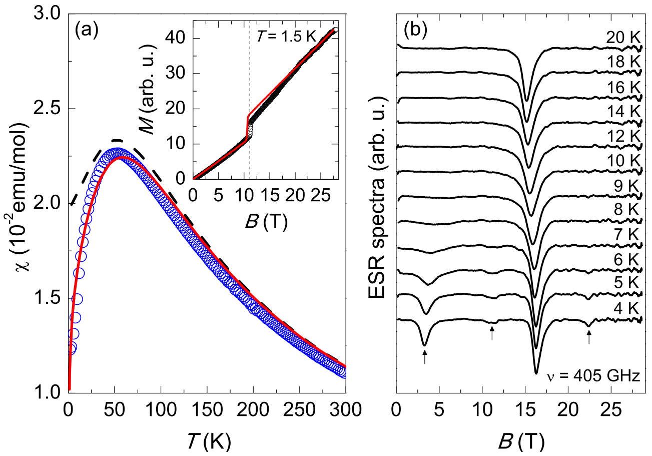

FIG. 2. (Color online) (a) Measured magnetic susceptibility (circles) and comparison to the quantum Monte Carlo (solid line) and the classical (dashed line) calculations for alternating $S = 5/2$ chain with $J_4/J_2 = 0.6$ and $J_2 = 16$ K. Inset: High-field magnetization measured at $T = 1.5$ K (circles) and the simulation to the model described in the text (solid line). The dashed line indicates the position of B_{SF}. (b) Temperature evolution of ESR spectra at 405 GHz for $B \,||\, b$. Arrows indicate antiferromagnetic resonance modes emerging below the Néel transition temperature.

Magnetic properties.– Quantum Monte Carlo simulations of the bulk magnetic susceptibility for alternating $S = 5/2$ chains with $L = 60$ sites were carried out with the ALPS 1.3 [20] directed loop application [21] in the stochastic series expansion framework [22]. For $J_2 = 16$ K and the DFT determined ratio $J_4/J_2 = 0.6$ we find a very good agreement between our simulations and the experimental data for $B = 0.1$ T and $B||b$ [Fig. 2(a)]. A rather good agreement is also achieved when classical spins are considered. However, since the tetramer model can also fit the susceptibility data [9], we need an independent experimental proof to discriminate between the two models and to fix the precise values of J's.

Magnetization measurements performed at $T = 1.5\,\mathrm{K}$ for B parallel to the ICM direction (b axis) show a linear increase of the magnetization with B and the existence of a clean step at around $B_{SF} = 11\,\mathrm{T}$ [inset in Fig. 2(a)]. Such a behavior is reminiscent of a spin-flop-like process, implying the presence of considerable magnetic anisotropy.

Electron spin resonance.– Magnetic anisotropies can be determined by electron spin resonance (ESR) [23–26], which in the magnetically ordered state allows a detection of collective low-energy magnetic excitations at $\mathbf{Q} = 0, \pm\,\mathbf{q}_{ICM}$ – the so-called antiferromagnetic resonance (AFMR) modes [27]. Measurements at fixed resonant frequencies for magnetic fields $B||b$ were performed at the Institute for Materials Research, Tohoku University, Sendai, Japan. In the paramagnetic state a strong ESR signal at $g = 2.005$ is observed, as expected for Fe^{3+} ($S = 5/2$) ions. At T_{N1} the paramagnetic signal disappears and is replaced by new resonances [marked by arrows in Fig. 2(b)] shifted with respect to the paramagnetic $g = 2.005$ value.

The new resonances below T_{N1} are attributed to AFMR modes. Resonant fields for individual AFMR lines strongly depend on the resonance frequency [Fig. 3(a)], allowing us to derive their frequency-field dispersions in the range 95 to 405 GHz and 0 to 30 T at 2 K [Fig. 3(b)]. The lowest and at the same time the most intense excitation mode marked by arrows in Fig. 3(a) shows a zero-field gap $\Delta\nu_{ZF} \sim 240\,\mathrm{GHz}$ [Fig. 3(b)] corroborating a sizable magnetic anisotropy and in agreement with high-field magnetization measurements. With increasing magnetic field the gap reduces to $\sim 100\,\mathrm{GHz}$ at B_{SF}, where the slope is reversed and the gap increases again with increasing field. In addition, at least five more high-frequency modes were detected [Figs. 2(b) and 3(a)], which also dramatically change their behavior at B_{SF}.

Simulations.– In order to relate the high-field magnetization and the AFMR results to DFT calculations the first step is to determine the magnetic ground state of the infinite spin lattice via minimizing the classical energy (compare secion S1) corresponding to the proposed Heisenberg model [Fig. 1(b)]. Since Fe^{3+} ions are in the high-spin $S = 5/2$ state, such a classical treatment of the model is reasonably justified. In our approach we assume coplanar ordering and fixed sizes of the magnetic moments thus ignoring their amplitude modulation established from neutron diffraction experiments [8]. Starting from the parameters obtained from the GGA+U calculations with U = 0 eV, 3 eV, and 5 eV (Table I), the solution immediately converges to an ICM order. For U = 3 eV the experimental $q^{y}_{ICM} = 0.463$ is reached by fine tuning of the interchain couplings, i.e., J_1, J_3, and J_6, up to 2 % (Table I). We note that using the tetramer model parameters, i.e., $|J_1| = |J_2| \sim |J_3| \gg |J_4|$, $|J_5|$, $|J_6|$ [9], we were unable to generate the ICM magnetic order, which clearly demonstrates that the tetramer model is inappropriate.

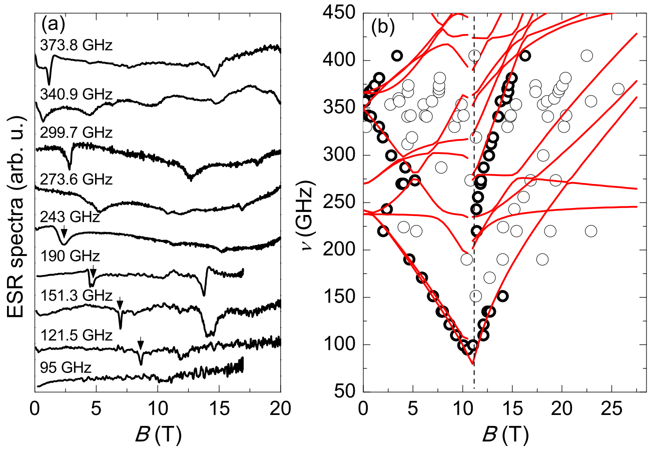

FIG. 3. (Color online) (a) Field dependence of AFMR spectra at 1.5 K for $B||b$ and various resonant frequencies between 95 and 405 GHz. (b) Frequency-field dependence for intense (thick circles) and weak (thin circles) AFMR modes. Solid lines are simulations to the model described in the text. The dashed line indicates B_{SF}.

Due to the excellent agreement with q^{y}_{ICM} we now use the optimized parameters (Table I, fourth column) to calculate the AFMR modes. For computing the equations of motion [23] we define a finite magnetic lattice comprising 7 unit cells coupled along the crystallographic b axis, i.e., mimicking the experimentally observed $q^{y}_{ICM} = 0.463 \sim 3/7$. We assume $5\,\mu_B$ for the size of Fe^{3+} moments and introduce an easy plane anisotropy, DS_z^2. Here D is the magnitude of single-ion anisotropy. To fix the direction of the hard axis along $z = (0.31, 0, 0.95)$ we take into the account the orientation of the ordered magnetic moments [8] and a two-fold screw axis, which coincides with the b axis. The only free parameters left in these calculations are thus D and the strength of the J_2 interaction (all other interactions are scaled appropriately).

The strongest AFMR mode is best described [Fig. 3(b)] by $J_2 = 19.0\,\mathrm{K}$ and $D = 0.18\,\mathrm{K}$ (Table I). We stress that the theoretical curve nicely reproduces the softening of this mode up to B_{SF} and its reversed character at higher fields. At the same time, the dispersions of all other intense higher-frequency AFMR modes are in convincing agreement with the experiment [Fig. 3(b)]. Moreover, the same set of parameters perfectly simulates the magnetization response to the applied magnetic field including the magnetization step at B_{SF} [inset in Fig. 2(a)]. To conclude this part, we emphasize a remarkable agreement between experiments and ratios of J's obtained by the DFT calculations for GGA+U with $U = 3\,\mathrm{eV}$ achieved only by scaling slightly the exchange interactions.

Discussion.– The main result of this study is the finding that $FeTe_2O_5Br$ has to be treated as a system of alternating $S=5/2$ chains weakly coupled by frustrated interactions, in contrast to the previously proposed tetramer model. The knowledge of the appropriate spin model allows us to investigate the ME mechanism from a microscopic perspective. In order to identify the exchange pathway responsible for the ME effect we first recall that q^y_{ICM} is temperature independent in the high-temperature ICM phase (between T_{N1} and T_{N2}), while in the low-temperature ICM phase (below T_{N2}) it scales similarly to the electric polarization, i.e., it behaves as $(T_{N2}-T)^{0.35}$ [11]. To address this important point we return to the minimization of the classical energy for the infinite lattice and calculate how q^y_{ICM} is affected by small changes of different J_i's. Since the ICM modulation is perpendicular to the alternating chains, it suffices to vary only the interchain exchange couplings J_i (i=1,3,5,6) with respect to the values that reproduce the AFMR modes at $T=2\,\mathrm{K}$. In order to reproduce the decrease of q^y_{ICM} observed below T_{N2}, J_1 has to be reduced, while J_3, J_5 and J_6 have to be increased (Fig. 4).

Given that J_1 and J_3 are superexchange interactions via Fe-O-Fe bridges, they are expected to behave according to Goodenough-Kanamori rules [15, 16]. If J_1 is responsible for the ME effect, then the Fe-O-Fe angle should be reduced or the Fe-O distance increased in order to weaken J_1. No significant structural changes for this bond have been observed in our high-resolution synchrotron x-ray diffraction experiments [8] (compare also section S3) thus ruling out this possibility. An analogous conclusion can be derived also for J_3. We are thus left with the two remaining candidates – J_5 and J_6 super-superexchange interactions – which both involve Te^{4+} ions. Since the only sizable change at the ME transition corresponds to the shortening of the Fe_2-Te_3 distance, involved in the J_5 pathway, we assign the microscopic origin of the ME coupling to the changes of this interaction. The key to understanding the ME effect is hidden in the low symmetry of the long Fe-O-Te-O-Fe bridges, which allows emergent magnetic order to provoke a softening of an appropriate phonon mode and hence a net electric polarization. We stress that this is possible even if the spin-orbit coupling is very small. This resembles $Ni_3V_2O_8$, where the magnetostriction mechanism is proposed to be responsible for the ME couping [28]. Finally, we point out that tellurite halide systems seem particularly inclined to such effects, since their long low-symmetry exchange bridges involve easily polarizable Te^{4+} lone-pair electrons, which enable that already minimal changes in the strength of the exchange interactions are sufficient to produce a measurable macroscopic effect.

Conclusions.– We have shown that the magnetic exchange network of the $FeTe_2O_5Br$ system should be regarded as a system of alternating Fe chains with weaker frustrated interchain interactions. Frustration is found to be responsible for the observed low-symmetry ICM magnetic ordering, essential for the establishment of the multiferroic phase. Additionally, we show that in $FeTe_2O_5Br$ the ME effect on the microscopic level originates from the magnetostriction of interchain J_5 Fe-O-Te-O-Fe exchange pathway, where the net electric polarization comes from the Te^{4+} lone-pair electrons. Finally, our findings clearly demonstrate that in tellurite halides one needs to be extremely cautious when making assumptions about the exchange network, as arguments based solely on the crystal structure may be very misleading. Long super-superexchange bridges involving Te^{4+} ions can lead to surprisingly strong interactions. In addition, their structural volatility makes the ME effect possible.

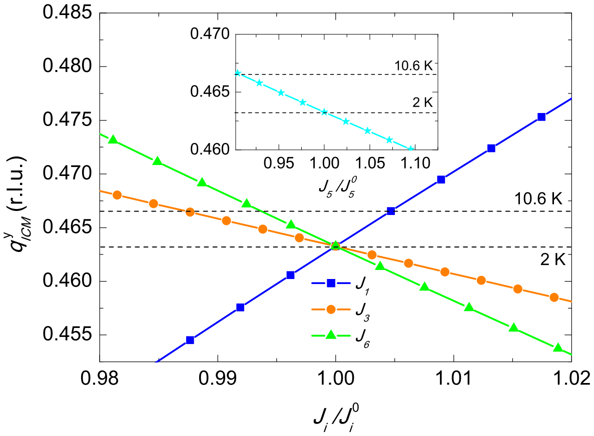

FIG. 4. (Color online) Dependence of q^y_{ICM} on interchain exchange coupling constants ratios, J_i/J_i^0 for $i=1,3,6$, calculated by direct minimization of the classical energy, where J_i^0 are exchange parameters used in AFMR simulations. Inset: the same dependence calculated for J_5.

We acknowledge help from the ESRF Swiss-Norwegian Beamline scientists D. Chernyshov and Ya. Filinchuk with the x-ray experiment and data analysis. This work has been supported by the Swiss National Science Foundation project 200021-129899, the DFG (SFB/TR 49 and HO 2325/4-2), and by the Helmholtz Association through HA216/EMMI, and the Slovenian research agency (J1-2118).

SUPPLEMENTARY INFORMATION

S1. Magnetic ground state calculations

We consider initially the simple Heisenberg model,

$$H = \sum_{i,j} J_{i,j} \vec{S}_i \cdot \vec{S}_j, \text{ where } J_{i,j}=J_1,\dots,J_6. \tag{1}$$

Due to the hard axis anisotropy, we will consider in what follows coplanar moments. In this case the classical energy can be written as a function of the angle θ_i

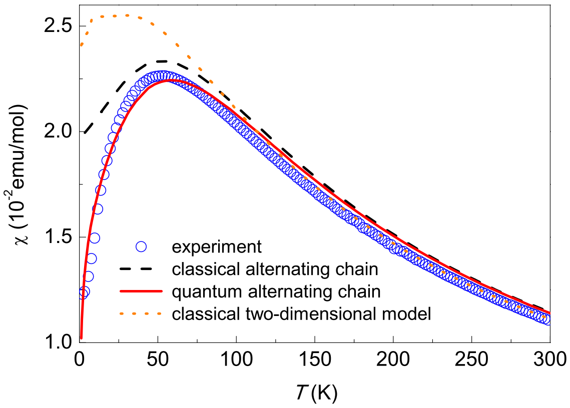

FIG. S1. (Color online) Measured magnetic susceptibility (circles), classical (dashed line) and quantum (solid line) Monte Carlo results for an alternating $S = 5/2$ chain with 60 spins, $J_4/J_2 = 0.6$, and $J_2 = 16$ K. Here we also include results for a two-dimensional 64×64 lattice of classical spins (dotted line), using the exchange ratios determined from the ground state minimization and AFMR calculations, but with $D = 0$ and scaled to $J_2 = 12$ K. Statistical errors of the Monte Carlo sampling procedure are well below the width of the lines.

corresponding to the orientation of the spin i with respect to the predetermined direction within the confined plane

$$E_{Cl} = S^2 \sum_{\langle i,j\rangle} J_{\langle i,j\rangle} \cos(\theta_j - \theta_i). \tag{2}$$

The classical energy thus depends only on the differences of orientations from spin to spin.

For a spiral order, E_{Cl} can be written as a function of 8 angles θ_i and the twist angles q^y and q^z defined as follows:

$$\begin{aligned} \theta_{i,(n+1)r_y+mr_z} &= \theta_{i,nr_y+mr_z} + q^y \\ \theta_{i,nr_y+(m+1)r_z} &= \theta_{i,nr_y+mr_z} + q^z, \end{aligned} \tag{3}$$

where n and m are the cell indices.

We used the conjugate gradient method to minimize the energy and to find the magnetic structure of the classical ground state.

S2. Magnetic susceptibility calculations

The magnetic susceptibility was computed by classical and quantum Monte Carlo simulations of the Heisenberg model (1) and compared to our single crystal $\chi(T)$ measurements for $B = 0.1$ T and $B||b$. Results for the alternating spin chain model were already presented in the main text; here we also present results for magnetic susceptibility of a two-dimensional lattice of classical spins with the exchange ratios determined from the ground state minimization and AFMR calculations (Fig. S1). In order to explain the observed high-temperature behavior within the two-dimensional model, we need to scale to $J_2 = 12$ K, while for simplicity we set $D = 0$. All numerical results are for a fixed system size and periodic boundary conditions, but we have checked that finite-size effects are negligible except possibly at very low temperatures. Theoretical results were converted to experimental units assuming a spectroscopic g-factor $g = 2$.

Inspired by the scaling of the high-temperature behavior with spin quantum number S, we used a phenomenological scaling

$$\chi_{S,\mathrm{phen}}(T) = \chi_{\mathrm{cl}}(S(S+1)\,T) \tag{4}$$

to map the classical result χ_{cl} to the quantum result for spin S. As is illustrated by the results for the alternating chain, this works well at high temperatures, but misses a suppression of χ by quantum fluctuations at low temperatures.

In the two-dimensional model, interchain coupling is frustrated. Since this gives rise to a sign problem in the quantum Monte Carlo approach, we have to rely exclusively on the classical Monte Carlo simulations for this case. The two-dimensional model fits the experimental magnetic susceptibility at high temperatures at least as well as the chain model, but the agreement is worse around and below the maximum of $\chi(T)$ (Fig. S1). However, we have to keep in mind that in analogy to

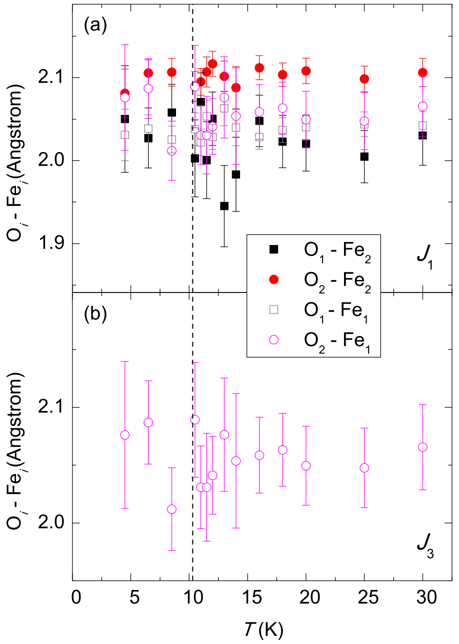

FIG. S2. Refinement results for the O-Fe distances obtained from synchrotron x-ray diffraction, corresponding to (a) J_1 and (b) J_3 exchange pathways.

the one-dimensional model, quantum fluctuations are expected to reduce $\chi(T)$ at low temperatures also in two dimensions. Furthermore, the frustrated nature of the interchain coupling might enhance this reduction. In any case, we attribute the fact that a one-dimensional model yields a good effective description to the frustration in the interchain coupling. Finally, we note that the two-dimensional model exhibits signatures of an ordering transition at $T \approx 9.5$ K. This is remarkably close to the experimentally observed ordering transitions, although the Mermin-Wagner theorem forbids a true finite-temperature ordering transition in a strictly two-dimensional Heisenberg model.

In conclusion, the fact that one-dimensional, two-dimensional and tetramer [9] models provide good fits to the magnetic susceptibility of $\mathrm{FeTe_2O_5Br}$ demonstrates that further data is needed to clarify the nature of the microscopic exchange network.

S3. Synchrotron x-ray diffraction

Low temperature single crystal X-ray synchrotron diffraction measurements were performed at the BM01A Swiss-Norwegian Beamline of ESRF (Grenoble, France). Data sets (typically 780 reflections per temperature point) were collected in the temperature range 4.5 K to 35 K at a wavelength of 0.64 Å, using a closed-cycle He cryostat mounted on a six-circle kappa diffractometer KUMA. Here we show refinement results for interatomic distances corresponding to interchain exchange pathways (Figs. S2, S3). The only significant changes occurring below $T_{N2} = 10.5\,\mathrm{K}$, involve Te_3, i.e., the J_5 exchange pathway.

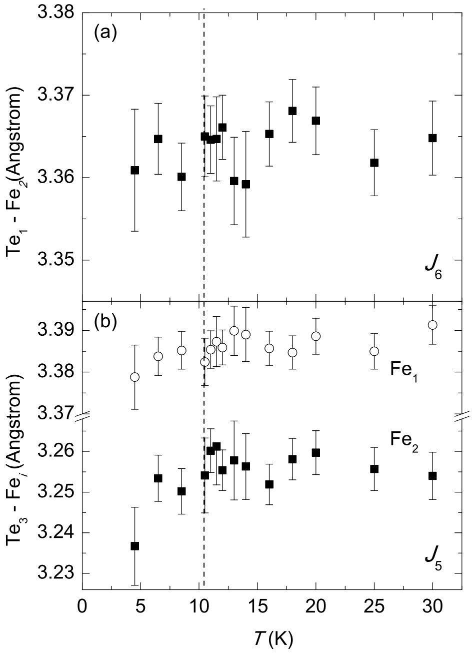

FIG. S3. Refinement results for the Fe-Te distances obtained from synchrotron x-ray diffraction, corresponding to (a) J_6 and (b) J_5 exchange pathways.

---

[1] *Introduction to Frustrated Magnetism*, edited by C. Lacroix, P. Mendels, and F. Mila (Springer-Verlag, Berlin, 2011).

[2] S.-W. Cheong and M. Mostovoy, Nature Mater. **6**, 13 (2007).

[3] D. Khomskii, Physics **2**, 20 (2009).

[4] W. Eerenstein, N. D. Mathur, and J. F. Scott, Nature **442**, 759 (2006).

[5] N. Hur, S. Park, P. A. Sharma, J. S. Ahn, S. Guha, and S.-W. Cheong, Nature **429**, 392 (2004).

[6] O. Zaharko, H. Rønnow, J. Mesot, S. J. Crowe, P. J. Brown, A. Daoud-Aladine, A. Meents, A. Wagner, M. Prester, H. Berger, and D. McK. Paul, Phys Rev. B **73**, 064422 (2006).

[7] H. Murakawa, Y. Onose, K. Ohgushi, S. Ishiwata, and Y. Tokura, J. Phys. Soc. Jpn. **77**, 043709 (2008).

[8] M. Pregelj , O. Zaharko, A. Zorko, Z. Kutnjak, P. Jeglič, P. J. Brown, M. Jagodič, Z. Jagličić, H. Berger, and D. Arčon, Phys. Rev. Lett. **103**, 147202 (2009).

[9] R. Becker, M. Johnsson, R. K. Kremer, H.-H. Klauss, and P. Lemmens, J. Am. Chem. Soc. **128**, 15469 (2006).

[10] R. Becker and M. Johnsson, J. Solid. State Chem. **180**, 1750 (2007).

[11] M. Pregelj, A. Zorko, O. Zaharko, Z. Kutnjak, M. Jagodič, Z. Jagličić, H. Berger, M. de Souza, C. Balz, M. Lang, and D. Arčon, Phys. Rev. B **82**, 144438 (2010).

[12] J. Deisenhofer, R. M. Eremina, A. Pimenov, T. Gavrilova, H. Berger, M. Johnsson, P. Lemmens, H.-A. Krug von Nidda, A. Loidl, K.-S. Lee, and M.-H. Whangbo, Phys Rev. B **74**, 174421 (2006).

[13] H. Das, T. Saha-Dasgupta, C. Gros, and R. Valentí, Phys Rev. B **77**, 224437 (2008).

[14] R. Valentí, T. Saha-Dasgupta, C. Gros, and H. Rosner, Phys Rev. B **67**, 245110 (2003).

[15] J. B. Goodenough, Phys. Rev. **100**, 564 (1955).

[16] J. Kanamori, J. Phys. Chem. Solids **10**, 87 (1959).

[17] K. Koepernik and H. Eschrig, Phys. Rev. B **59**, 1743 (1999); `http://www.FPLO.de`.

[18] O. K. Andersen and T. Saha-Dasgupta, Phys. Rev. B **62**, R16219 (2000).

[19] H. O. Jeschke, I. Opahle, H. Kandpal, R. Valentí, H. Das, T. Saha-Dasgupta, O. Janson, H. Rosner, A. Brühl, B. Wolf, M. Lang, J. Richter, S. Hu, X. Wang, R. Peters, T. Pruschke, and A. Honecker, Phys. Rev. Lett. **106**, 217201 (2011).

[20] A. F. Albuquerque, F. Alet, P. Corboz, P. Dayal, A. Feiguin, S. Fuchs, L. Gamper, E. Gull, S. Gürtler, A. Honecker, R. Igarashi, M. Körner, A. Kozhevnikov, A. Läuchli, S. R. Manmana, M. Matsumoto, I. P. McCulloch, F. Michel, R. M. Noack, G. Pawłowski, L. Pollet, T. Pruschke, U. Schollwöck, S. Todo, S. Trebst, M. Troyer, P. Werner, and S. Wessel, J. Magn. Magn. Mater. **310**, 1187 (2007).

[21] F. Alet, S. Wessel, and M. Troyer, Phys. Rev. E **71**, 036706 (2005).

[22] O. F. Syljuåsen and A. W. Sandvik, Phys. Rev. E **66**, 046701 (2002).

[23] M. Pregelj, A. Zorko, H. Berger, H. van Tol, L. C. Brunel, A. Ozarowski, S. Nellutla, Z. Jagličić, O. Zaharko, P. Tregenna-Piggott, and D. Arčon, Phys. Rev. B **76**, 144408 (2007).

[24] A. Zorko, M. Pregelj, A. Potočnik, J. van Tol, A. Ozarowski, V. Simonet, P. Lejay, S. Petit, and R. Ballou, Phys. Rev. Lett. **107**, 257203 (2011).

[25] M. Herak, A. Zorko, D. Arčon, A. Potočnik, M. Klanjšek, J. van Tol, A. Ozarowski, and H. Berger, Phys. Rev. B **84**. 184436 (2011).

[26] A. Zorko, S. Nellutla, J. van Tol, L. C. Brunel, F. Bert, F. Duc, J.-C. Trombe, M. A. de Vries, A. Harrison, and P. Mendels, Phys. Rev. Lett. **101**, 026405 (2008).

[27] D. Hüvonen, U. Nagel, T. Rõõm, Y. J. Choi, C. L. Zhang, S. Park, and S.-W. Cheong, Phys. Rev. B **80**, 100402(R) (2009).

[28] A. B. Harris, T. Yildirim, A. Aharony, and O. Entin-Wohlman, Phys. Rev. B **73** 184433 (2006).